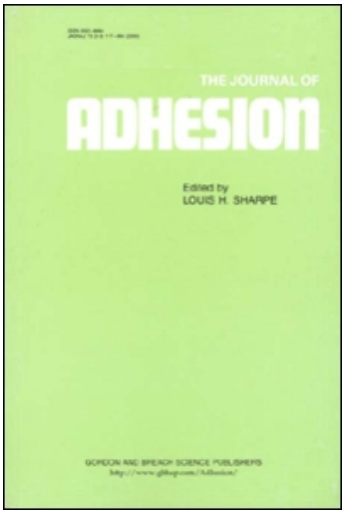

The Journal of Adhesion
Publication details, including instructions for authors and subscription information:
http://www.informaworld.com/smpp/title~content=t713453635

Influence of Hydrogen Bonding on the Adhesive Properties of Photo-Curable Acrylics

Matthew P. Cashion[a]; Taigyoo Park[a]; Timothy E. Long[a]
[a] Department of Chemistry, Macromolecules and Interfaces Institute, Virginia Tech, Blacksburg, VA, USA

To cite this Article Cashion, Matthew P. , Park, Taigyoo and Long, Timothy E.(2009) 'Influence of Hydrogen Bonding on the Adhesive Properties of Photo-Curable Acrylics', The Journal of Adhesion, 85: 1, 1 — 17
To link to this Article: DOI: 10.1080/00218460902727332
URL: http://dx.doi.org/10.1080/00218460902727332

The Journal of Adhesion, 85:1–17, 2009

ISSN: 0021-8464 print/1545-5823 online
DOI: 10.1080/00218460902727332

Taylor & Francis
Taylor & Francis Group

Influence of Hydrogen Bonding on the Adhesive Properties of Photo-Curable Acrylics

Matthew P. Cashion, Taigyoo Park, and Timothy E. Long
Department of Chemistry, Macromolecules and Interfaces Institute, Virginia Tech, Blacksburg, VA, USA

Novel hot melt pressure sensitive adhesives (HMPSAs) were developed from acrylic terpolymers of 2-ethylhexyl acrylate (EHA), hydroxyethyl acrylate (HEA), and methyl acrylate (MA) functionalized with hydrogen bonding and photo-reactive functionalities. The hydrogen bonding and photo-reactive sites were introduced from the reaction of HEA repeat units with cyclohexyl isocyanate and cinnamoyl chloride, respectively. The functionalization reaction conditions were optimized to tailor the degree of urethane and cinnamate groups in order to examine the influence of hydrogen bonding and photo-active groups in low T_g acrylics. The synergy of hydrogen bonding and photo-reactivity resulted in higher peel values and rates of cinnamate photo-reactivity with increasing urethane concentration. The increase in cinnamate photo-reactivity with increasing urethane concentration provides evidence that hydrogen bond associations can promote cinnamate dimerization. Isothermal rheological experiments conducted at 150°C confirmed the melt stability of the cyclohexyl urethane linkage, cinnamate, and the acrylic composition indicating the potential for hot melt adhesive applications.

Keywords: Adhesives; Cinnamate; Crosslinking; Hydrogen bonding; Photochemistry; Urethane

INTRODUCTION

Pressure sensitive adhesives (PSAs) bond to a variety of substrates with very low pressure applied for short periods [1]. PSAs are widely used in electronic devices, tapes, labels, medical devices, and the automotive industry [1–3]. PSA formulations are soft materials that are

Received 15 September 2008; in final form 19 November 2008.
Presented in part at the 29th Annual Meeting of The Adhesion Society, inc., in Jacksonville, Florida, USA, 19–22 Februart 2006.
Address correspondence to Timothy E. Long, Department of Chemistry Virginia Tech (0212), Blacksburg, VA 24061, USA. E-mail: telong@vt.edu

inherently tacky at room temperature, and the viscoelastic nature of the adhesive defines the balance between adhesive and cohesive performance. Sufficient adhesive performance requires adequate mechanical strength to resist creep and prevent cohesive failure.

PSAs applied in the molten state in the absence of solvent are termed hot melt pressure sensitive adhesives (HMPSAs) [3]. The exclusion of solvent makes HMPSAs more economically and environmentally advantageous and, furthermore, application in the melt increases production efficiency and eliminates drying steps, reducing energy consumption. HMPSAs are designed to provide tack without the use of activators such as water, solvent, or heat. The bulk properties that make HMPSAs desirable for processing also limit their adhesive performance [4]. Low viscosities are required at processing temperatures and during application to facilitate spreading and intimate contact with the substrate. Adhesive performance is inferior at molecular weights that are suitable for melt processing due to insufficient chain entanglements. Molecular cohesion is a material's internal resistance to failure, and the mechanical and physical properties of adhesives are dependent upon chain cohesion [5,6]. Post processing strategies to increase molecular weight and cohesion include covalent crosslinking [7,8], physical crosslinking [4,9–11], and the addition of tackifiers [12].

Future strategies are required to incorporate the desirable properties of acrylic HMPSAs exploiting facile synthetic procedures. Acrylics offer a wide application temperature, resistance to oxidation and UV-light degradation, optical clarity, and long-term durability [13]. Moreover, acrylic formulations exhibit adhesive properties without the use of additives. This manuscript describes the photo-curing of associated acrylic architectures for HMPSA applications. The association of macromolecules through noncovalent interactions is accomplished through functionality that facilitates the formation of ionic interactions [9], donor-acceptor complexes [14], hydrogen bonding [15], liquid crystalline behavior [16], and the self-assembly of amphiphilic polymers [17]. Hydrogen bonding is a versatile scaffold for noncovalent associations. Hydrogen bonding functionality is prevalent in biological systems, readily accessible in rational synthesis, and the associations are reversible.

Association of hydrogen bonding groups provides a method to increase the apparent molecular weight after application, and temperatures above the hydrogen bonding dissociation temperature result in low viscosities for melt processing. Poly(acrylic acid) (PAA) is the most published source of hydrogen bonding functionality incorporated in PSA formulations [7,18]. Hydrogen bonding between carboxylic

groups forms cyclic dimers, or linear associations, in a *face-on* or lateral fashion [19]. However, PAA can thermally crosslink, and intermolecular anhydrides form at temperatures greater than 150°C [20]. Crosslinking during processing is not desirable in hot melt applications, and acrylic acids offer only limited utility.

Hydrogen bonding urethane functionality is commonly used for curing PSA precursors [21,22]. Asahara *et al*. [23] crosslinked poly-[ethyl acrylate (EA)-*co*-2-ethylhexyl acrylate (EHA)-*co*-2-hydroxyethyl methacrylate (HEMA)] random copolymers with an isocyanate end-capped urethane oligomer. Reaction of the primary hydroxyl groups of HEMA with the isocyanate functionalized oligomer developed a network structure. The urethane groups were incorporated exclusively during crosslinking, and the consumption of isocyanate groups correlated to the degree of crosslinking. The peel performance depended upon the duration and temperature of curing, as well as on the crosslinker concentration. Asahara and coworkers concluded that lower urethane concentrations yielded higher peel strengths.

Functionality that facilitates electron beam [24] or photo-crosslinking [25] are popular curing strategies for HMPSAs. Photo-curing is a prevalent crosslinking mechanism that is employed to increase the molecular weight and cohesive strength of HMPSAs. Photo-curing associated macromolecular architectures has received significant interest in the layer-by-layer (LBL) assembly of multilayer thin films [26], formation of supramolecular nanostructures [27], and formation of liquid crystalline polymers [28]. Recently, methacrylate photo-active groups were incorporated at the periphery of well-defined four-arm star-shaped poly(D,L-lactide)s and photo-crosslinked, producing biologically compatible networked films [29,30]. Photo-curing offers solvent-free processes, rapid rates of crosslinking, and does not require drying steps, which suggests an economical and efficient process. Crosslinking occurs only during UV-exposure, therefore, controlling the degree of crosslinking with UV-dose. The crosslinker concentration and composition determine the mechanical and adhesive properties of HMPSAs.

Conventional photo-curable strategies employ chain-like reactions initiated with reactive radicals [5,31] or cations [32]. Chain-like reactive groups typically absorb at high-energy wavelengths. Photo-initiators that absorb at longer wavelengths are utilized to limit exposure to high energy light and reduce the energy requirements for curing. Homogeneous curing of chain-like photo-crosslinking reactions is difficult due to the limited diffusion of the photo-initiator and oxygen inhibition. In the 1950's, Robertson *et al.* were the first to study the photo-dimerization of cinnamate groups [33]. Robertson *et al.*

reported the photo-initiated crosslinking reaction of cinnamate groups in poly(vinyl cinnamate). The photochemistry of cinnamates involves two photo-reactions upon UV-irradiation, *i.e.*, the trans-cis isomerization and photo-dimerization [34]. Photo-dimerization involves the $[2\pi + 2\pi]$ cycloaddition of cinnamates in the head-to-head or head-to-tail configuration to form cyclobutane. Other photo-reactive groups that photo-dimerize in a $[2\pi + 2\pi]$ cycloaddition include furans [35], maleimides [36], chalcones [37], and coumarins [38]. Since Robertson's initial discovery, the cinnamate functionality has received interest in polymeric and low molar mass reactions as a robust chromophore capable of photo-dimerizing in the presence of oxygen [39].

In this study, low T_g acrylic random copolymers were functionalized with urethane and cinnamate functionalities to introduce a novel combination of hydrogen bonding and photo-curable substituents, respectively. To the best of our knowledge, there is not a literature precedence describing the use of hydrogen bonding and cinnamate photo-active groups in the development of acrylic HMPSAs. The degree of urethane and cinnamate functionality was varied to systematically study the adhesive and mechanical properties as a function of composition.

EXPERIMENTAL

Materials

The composition of Precursor Copolymer 1 contained poly(EHA)-*co*-hydroxyethyl acrylate (HEA) (82-18 mol%). Precursor terpolymer 2 contained poly[EHA-*co*-HEA-*co*-methyl acrylate (MA)] (60-24-16 mol%), and Precursor Terpolymer 3 contained poly(EHA-*co*-HEA-*co*-MA) (64-14-22 mol%). Avery Dennison (Mill Hall, PA, USA) provided Precursor Copolymers 1, 2, and 3. Tetrahydrofuran (THF), toluene, cinnamoyl chloride, cyclohexyl isocyanate, and triethylamine were received from Aldrich (Milwaukee, WI, USA). Cinnamoyl chloride was sublimed producing white crystals and cyclohexyl isocyanate was used without further purification. Triethylamine was distilled from CaH_2. Reagent grade THF was passed through a PURE SOLV MD-3 Solvent Purification System (Innovative Technology, Inc., Newburyport, MA, USA) immediately prior to use. All reactions were purged with argon and performed under an argon atmosphere in flame-dried glassware.

Instrumentation

Size exclusion chromatography (SEC) was performed on a Waters (Milford, MA, USA) instrument equipped with 3 in-line Polymer

Laboratories PLgel 5-μm MIXED-C columns with a Waters 717 autosampler. SEC characterization was conducted at 40°C in THF (ACS grade) at a flow rate of 1 mL/min. A triple detection system included a Waters 2414 refractive index detector, Viscotek (Houston, TX, USA) 270 Dual Detector viscometer, and Wyatt Technologies (Santa Barbara, CA, USA) miniDAWN multiangle laser light scattering (MALLS) detector. Refractive index increments (dn/dc) values were determined online. Reported molecular weights were calculated from light scattering.

^{1}H NMR spectroscopy was performed on a Varian (Palo Alto, CA, USA) Unity 400 MHz spectrometer in $CDCl_3$ at 25°C. Differential scanning calorimetry (DSC) was performed on a TA Instruments (New Castle, DE, USA) DSC 1000 under a nitrogen flush at a heating rate of 10°C/min. The glass transition temperature (T_g) was determined as the midpoint of the glass transition endotherm of the second heat cycle. FTIR spectroscopy was performed on a MIDAC M-1700 FTIR (Costa Mesa, CA, USA) with Durascope single bounce diamond ATR. An Analytical Instrument Systems, Inc. (Flemington, NJ, USA) UV-spectrometer equipped with fiber optic cables, a DT1000CE light source, and an Ocean Optics USB2000 UV-Vis (Ocean Optics, Dunedin, FL, USA) detector was used to determine the rate of cinnamate photo-dimerization.

Synthesis of Cinn1, Cinn2, and Cinn3: Cinnamate Functionalization of Precursors 1–3

The precursor (15 g) was dissolved in THF (60 g, 20 wt%) in a 250-mL round-bottomed two-neck flask equipped with a magnetic stir bar. Cinnamoyl chloride, in a 1:1 molar equivalence to HEA in the precursor, was added to a 50-mL round-bottomed flask covered with aluminum foil and dissolved in THF (10 mL, 0.120 mol). Triethylamine, in a 1:1 molar equivalence to cinnamoyl chloride, was added to the reaction flask using a purged syringe. Next, the reaction flask was covered in aluminum foil and equipped with an addition funnel that was wrapped in aluminum foil. The reaction flask was placed in an ice bath. The cinnamoyl chloride solution was introduced into the addition funnel using a degassed syringe. The cinnamoyl chloride solution was added drop-wise to the reaction flask at 0°C. The reaction continued to stir at 0°C for 2 h, and the product was finally precipitated into methanol and vacuum dried. The cinnamate-functionalized copolymers were characterized with ^{1}H NMR, IR, SEC, and DSC.

Synthesis of Ureth2: Urethane Functionalization of Precursor 2

Precursor 2 (20 g) was dissolved in toluene (30 g, 40 wt%) in a 250-mL round-bottomed flask equipped with a magnetic stir bar. Next, cyclohexyl isocyanate was added in the desired molar ratio compared with HEA, and 0.2 mL of 1 wt% di-*n*-butyltin-dilaurate in toluene was added. The charged molar ratio of cyclohexyl isocyanate to HEA depended on the desired degree of urethane functionalization. A condenser was attached and the reaction was conducted at 50°C for 8 h. After 8 h, the reaction mixture was precipitated into methanol and the precipitant was vacuum dried. Ureth2 was characterized with ^{1}H NMR, IR, SEC, and DSC.

Synthesis of Urethcinn2: Cinnamate Functionalization of Ureth2

Figure 1 displays the urethane and cinnamate functionalization of Precursor 2. Ureth2 (15 g) was dissolved in THF (60 g, 20 wt%) in a 250-mL round-bottomed two neck flask equipped with a magnetic stir bar. Cinnamoyl chloride, in a 10:1 molar equivalence to HEA of Ureth2, was added to a 50-mL round-bottomed flask covered with aluminum foil and dissolved in THF (10 mL, 0.120 mol). Triethylamine, in a 1:1 molar equivalence to cinnamoyl chloride, was added to the reaction flask using a purged syringe. Next, the reaction flask was covered

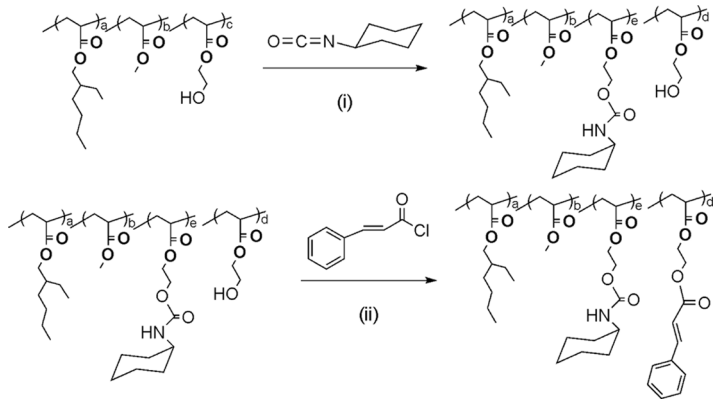

FIGURE 1 Synthesis of UrethCinn2, the urethane, and cinnamate functionalization of Precursor 2, (i) 0.2 mL of 1 wt% di-n-butyltin-dilaurate in toluene, 40 wt% solids in toluene, 50°C, (ii) triethylamine, 20 wt% solids in THF, 0°C.

in aluminum foil and equipped with an addition funnel that was wrapped in aluminum foil. The reaction flask was placed in an ice bath. The cinnamoyl chloride solution was introduced into the addition funnel using a degassed syringe. The cinnamoyl chloride solution was added drop-wise to the reaction flask at 0°C. The reaction continued to stir at 0°C for 2 h, and the product was finally precipitated into methanol and vacuum dried. UrethCinn2 was characterized with ^{1}H NMR, IR, SEC, and DSC.

Peel Analysis

The functionalized acrylic (10 g) copolymer was dissolved in toluene (15 g, 40 wt%). A foot-long strip of 8-in. wide backing paper was cleaned with acetone and isopropanol and heated to 80°C for 30 min. The functionalized acrylic film was drawn in a controlled manner on the backing paper using a 3 in. (7.6 cm) wide doctor blade to an average thickness of 21 μm. The film was placed in the oven at 80°C for 30 min. and ramped to 120°C for 5 min. Irradiated samples were cured at 10 ft/min. (25.4 cm/min) on a Fusion UV (Gaithersburg, MD, USA) model LC-6B benchtop conveyor equipped with a 100 W high pressure mercury lamp. Light intensities were measured using an EIT, Inc. (Sterling, VA, USA) UV power puck. UV-dosages were measured at UVA: $0.181 \pm .013\,J/cm^2$ and UVB: $0.147 \pm 0.05\,J/cm^2$ for 10 s of irradiation. Peel analysis was performed on a ChemInstruments Adhesion/Release Tester AR-1000 (Fairfield, OH, USA). Films were cut into 0.75 in. (1.9 cm) widths, and pressed onto ChemInstrument, Inc. 2×8 in. (5.1×20.3 cm) stainless steel plates with a 1 kg rubber roller. The 90° peel test were performed at 25°C at a rate of 12 in/min (30.5 cm/min). Reported peel values are an average of five tapes per sample. Peel values are reported in lb_f/in (g/cm), corresponding to the peeling force per width of tape.

Rate of Cinnamate Photo-dimerization and Gel Fraction Analysis

A quartz slide (1×1 inch) (2.5×2.5 cm) was washed with acetone, isopropanol, and THF. The control, or urethane sample (0.96 g), was dissolved in toluene (8.64 g) at 10 wt%. The solution was spin cast onto a square quartz slide (1×1 inch) (2.5×2.5 cm) at 2000 rpm for 1 min. The UV-Vis absorbance of the film was measured before UV-exposure. The coated slide was then irradiated for 10, 30, 60, 90, 120, 150, 180, 210, 240, and 270 s and the UV-Vis absorbance was measured after each exposure. Gel fractions were determined for UV-cured and

non-cured films. Soxhlet extraction was performed in refluxing THF for 12 h on UV-cured films irradiated for 10 s and non-cured films.

RESULTS AND DISCUSSION

Synthesis and Peel Performance of Cinn1, Cinn2, and Cinn3

The composition of the precursor copolymers included EHA, HEA, and MA. EHA was included to provide a low T_g segment for increased tack, HEA provided a functionalizable site, and MA provided a higher T_g segment to decrease the molecular weight necessary to achieve chain entanglements and provide increased cohesive strength [40]. Table 1 compares the composition, molecular weight, and T_g of acrylic Precursors 1–3. The compositions were tailored for a T_g of -50°C and M_w of 100,000.

All three precursors were functionalized with cinnamate groups to explore HEA's reactivity as a function of composition. All precursors were functionalized with cinnamate groups from the acid chloride reaction of HEA repeating units with cinnamoyl chloride. Characterization following cinnamate functionalization was performed using NMR spectroscopy, FTIR, DSC, and SEC analysis. ^{1}H NMR analysis of the cinnamate functionalized precursor confirmed the appearance of cinnamate resonances at 6.51, 7.38, 7.57, and 7.73 ppm. The resonance at 3.78 ppm corresponding to the methylene adjacent to the ester of HEA units diminished, and a new resonance at 4.35 ppm corresponding to the methylene adjacent to the ester of cinnamoyloxyethyl acrylate (CEA) appeared. Following cinnamate functionalization, the FTIR spectrum displayed characteristic cinnamate bands at 1637 and 980 cm^{-1}, corresponding to the cinnamates vinyl C=C stretching vibration and *trans*-vinylene C-H deformation [41]. Cinnamate functionalization resulted in an average molecular weight increase of 36%, despite all efforts to avoid spurious light; the molecular weight increase was attributed to premature intermolecular dimerization of the cinnamate sites. As expected, the T_g of all samples increased following cinnamate functionalization due to the incorporation of planar bulky cinnamate groups.

TABLE 1 Composition, Molecular Weight, and T_g Comparison of Precursors 1–3

Precursor	EHA (mol%)	HEA (mol%)	MA (mol%)	M_w (PDI)	T_g (°C)
1	82	18	–	111,000 (2.81)	−50
2	60	24	16	114,000 (2.59)	−44
3	64	14	22	105,000 (2.04)	−45

TABLE 2 Composition, Molecular Weight, and UV-Cured 90° Peel Strength of Cinn1, Cinn2, and Cinn3

Sample name	EHA (mol%)	HEA (mol%)	MA (mol%)	CEA (mol%)	M_w (PDI)	UV-Irradiated Peel (lb_f/in)*	Stdev
Cinnl	82	12	–	6	158,000 (3.91)	0.199	0.006
Cinn2	60	13	16	11	141,000 (5.18)	0.477	0.006
Cinn3	64	9	22	5	148,000 (2.00)	0.167	0.004

*lb/in × 178.6 = g/cm.

The reactivity of HEA's primary hydroxyl groups was examined as a function of precursor composition. A molar equivalence of cinnamoyl chloride to HEA for each precursor was charged. Precursor 2 achieved the highest degree of functionalization, with 46% of HEA groups reacting to form CEA. Precursor 1 only converted 33% of HEA groups to CEA, corresponding to the lowest degree of functionalization, and 36% of HEA groups in Precursor 3 were reacted to form CEA. The degree of HEA functionalization directly correlated to the concentration of bulky EHA units. Precursor 1 contained 82 mol% EHA and Precurson 2 possessed 60 mol% EHA, indicating the bulky EHA groups sterically hindered the reactivity of HEA hydroxyl groups.

Table 2 displays the UV-cured 90° peel strength of Cinn1, Cinn2, and Cinn3. UV-dosage was held constant for each film, and Cinn1, Cinn2, and Cinn3 had average film thicknesses of 20 ± 3, 22 ± 2, and $21 \pm 4\,\mu m$, respectively. Cinn2 exhibited the highest peel value of $0.477\,lb_f$/in (85.2 g/cm), and Cinn3 exhibited the lowest peel value of $0.167\,lb_f$/in (29.8 g/cm). All UV-cured samples failed adhesively, and non-cured films failed cohesively. The difference in failure mode between cured and non-cured films indicated intermolecular cinnamate crosslinking occurred during UV-exposure increasing the molecular weight and cohesive strength.

Hydrogen Bonding and Photo-Active Sites in Low T_g Acrylics

Precursor 2 was functionalized with urethane ($2U_{24}$) or cinnamate ($2C_{24}$) groups. $2U_{24}$ indicates 100% of HEA groups were functionalized with cyclohexyl isocyanate and $2C_{24}$ designates 100% of HEA groups were reacted with cinnamoyl chloride, and NMR spectroscopy confirmed that residual HEA units did not remain in the copolymers. Following complete urethane functionalization ($2U_{24}$) the M_w was 145,000 (2.08) and T_g −18°C. Adhesive $2C_{24}$ had a M_w of 188,000 (3.08) and T_g of −30°C.

Precursor 2 was functionalized with both urethane and cinnamate groups to investigate the influence of hydrogen bonding sites on the peel performance and cinnamate photo-reactivity. Optimized reaction conditions afforded the opportunity to incorporate cinnamate and urethane groups in the same precursor and control the degree of functionalization, as shown in Figure 1. The composition, molecular weight, and T_g of the urethane series are displayed in Table 3. Urethane functionalization was conducted at 50°C for 8 h, and the molar equivalence of cyclohexyl isocyanate charged determined the degree of urethane functionalization. For example, charging a ten molar excess of cyclohexyl isocyanate relative to HEA achieved 100% functionalization. Cinnamate functionalization was conducted for 2 h at 0°C, and complete cinnamate functionalization was achieved with a ten molar excess of cinnamoyl chloride to residual HEA units.

For hot melt applications, it is essential that the photocrosslinker and PSA composition are melt stable. The cinnamate chromophore is thermally stable to 200°C [42]. Cyclohexyl carbamate was incorporated as hydrogen bonding functionality due to its lack of UV-light absorption and excellent thermal stability. Figure 2 displays the isothermal melt rheology of $2U_{21}C_3$ at 150°C for 2 h. The complex viscosity was constant over the entire time range, which indicated the melt stability of the acrylic composition.

The UV-cured and non-cured peel analysis and failure modes of the urethane series are displayed in Table 4. The UV-cured and non-cured peel strengths of $2U_{24}$ were within error at 1.22 ± 0.159 lb_f/in (218 g/cm) and 1.34 ± 0.147 lb_f/in (239 g/cm), respectively, and exhibited the same mode of failure, indicating the cyclohexyl urethane linkage and PSA composition were UV-stable. $2U_{21}C_3$ displayed the largest UV-cured and non-cured peel values, 1.03 lb_f/in. (184 g/cm) and 1.64 lb_f/in. (293 g/cm), respectively. The

TABLE 3 Composition, Molecular Weight, and T_g of the Urethane Series [UEA: 2-(Cyclohexylcarbamoyloxy)Ethyl Acrylate (Urethane Ethyl Acrylate)]

Sample name	EHA (mol%)	MA (mol%)	UEA (mol%)	CEA (mol%)	M_w (PDI)	T_g (°C)
$2C_{24}$	60	16	–	24	188,000 (3.08)	−30
$2U_8C_{16}$	60	16	8	16	129,000 (4.59)	−27
$2U_{12}C_{12}$	60	16	12	12	152,000 (3.39)	−25
$2U_{17}C_7$	60	16	17	7	136,000 (3.56)	−23
$2U_{21}C_3$	60	16	21	3	150,000 (4.30)	−21
$2U_{24}$	60	16	24	–	145,000 (2.08)	−18

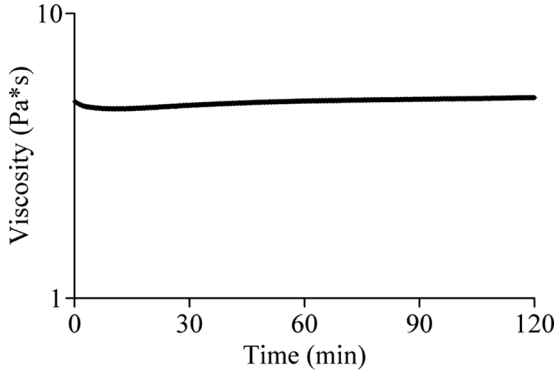

FIGURE 2 Isothermal melt rheology of $2U_{21}C_3$ at 150°C for 2 h.

UV-cured peel strength decreased as the concentration of cinnamate increased, resulting from an increased crosslink density elevating the modulus and T_g, which prevented the adhesive from spreading on the substrate [3]. All UV-cured tapes containing cinnamate groups failed 100% adhesively. Complete adhesive failure of the UV-cured films was attributed to the intermolecular dimerization of cinnamate groups leading to an increased molecular weight and network structure formation. The degree of adhesive failure for non-cured tapes was dependent upon the concentration of urethane functionality. As the degree of urethane functionality increased, the percentage of adhesive failure increased. Non-cured $2C_{24}$, which did not contain urethane sites, failed 100% cohesively, and $2U_{24}$, which contained only urethane functionality, exhibited the highest non-cured proportion of adhesive failure, 50%. Increasing adhesive failure with urethane concentration was attributed to an increase in apparent molecular weight resulting from the association of hydrogen bonding urethane groups.

TABLE 4 UV-Cured and Non-Cured 90° Peel Strength of the Urethane Series

Sample name	UV-irradiated peel (lb_f/in)	Stdev	Failure mode	Non-cured peel (lb_f/in)*	Stdev	Failure mode
$2C_{24}$	0.418	0.016	100% adhesive	0.844	0.008	100% cohesive
$2U_8C_{I6}$	0.731	0.014	100% adhesive	1.59	0.028	85% cohesive
$2U_{12}C_{12}$	0.855	0.017	100% adhesive	1.49	0.021	75% cohesive
$2U_{21}C_3$	1.03	0.026	100% adhesive	1.64	0.013	60% cohesive
$2U_{24}$	1.22	0.159	50% cohesive	1.34	0.147	50% cohesive

*lb/in × 178.6 = g/cm.

Influence of Hydrogen Bonding Sites on the Rate of Cinnamate Photo-Dimerization

Figure 3 displays the structure and composition of the urethane and control series. The control series consisted of Precursor 2 functionalized only with cinnamate sites, with residual HEA groups remaining. The compositions of the urethane and control series had comparable concentrations of cinnamate groups in order to investigate the influence of hydrogen bonding groups on the rate and efficiency of cinnamate photo-reactivity. Both the urethane and control series contained 60 mol% EHA and 16 mol% MA.

UV-vis spectroscopy was used to investigate the influence of hydrogen bonding associations on the rate of cinnamate photo-reactivity in the solid state. Urethane and control series films were spin coated on quartz slides from 10 wt% solutions in toluene, to a thickness of $1.0 \pm 0.14\,\mu m$. The films were spin cast to control film thickness and uniformity. The cinnamate chromophore absorbs 275 nm light, as seen in Figure 4 for $2U_{21}C_3$. Neither Precursor 2 nor $2U_{21}H_3$, 21 mol% urethane and 3 mol% HEA, absorbed UV-light. Urethane and control films were exposed to UV-light for periods of 10, 30, 60, 90, 120, 150, 180, 210, 240, and 270 s. Decreasing cinnamate UV-absorbance was monitored with an increase in UV-exposure. The decrease in cinnamate absorbance with increasing UV-exposure was attributed to the

Urethane Series				Control Series			
Sample name	UEA (mol%)	CEA (mol%)	T_g (°C)	Sample name	HEA (mol%)	CEA (mol%)	T_g (°C)
$2U_{21}C_3$	21	3	-21	$2H_{21}C_3$	21	3	-40
$2U_{12}C_{12}$	12	12	-25	$2H_{12}C_{12}$	12	12	-37
$2U_8C_{16}$	8	16	-27	$2H_9C_{15}$	9	15	-34

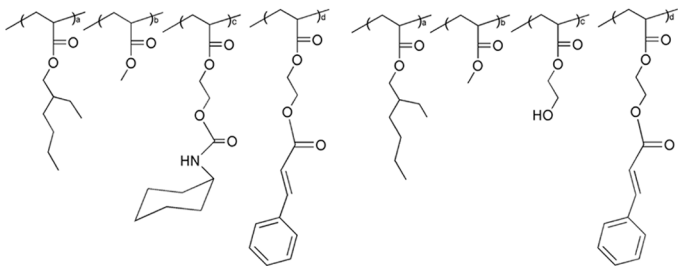

FIGURE 3 Composition and structure of the urethane and control series. Both the urethane and control series contained 60 mol% EHA and 16 mol% MA.

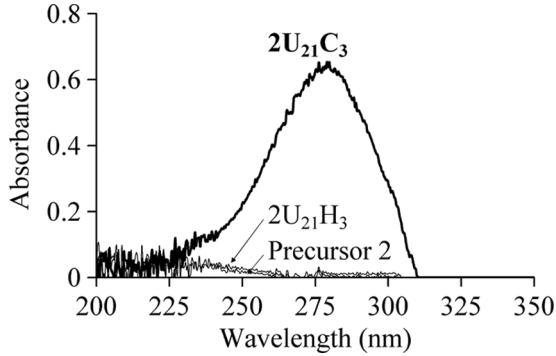

FIGURE 4 UV-vis absorbance of Precursor 2 following urethane functionalization ($2U_{21}H_3$) and cinnamate functionalization ($2U_{21}C_3$).

disappearance of conjugated cinnamate groups that photo-dimerized to form cyclobutane.

The rate of cinnamate dimerization was determined from a second order kinetic plot of absorbance *versus* UV-exposure time, as shown in Figure 5. $2U_{21}C_3$ contained the largest concentration of urethane groups and exhibited the fastest rate of cinnamate dimerization, $0.314\,s^{-1}$. The UV-absorbance for $2U_{21}C_3$ plateaued after 120 s of irradiation where 90% of cinnamate groups had photo-dimerized, and with increased UV-exposure further change in cinnamate absorbance was not observed. The plateau phenomenon was attributed to a steady-state concentration of cinnamate groups, resulting from the network of intermolecular cinnamate

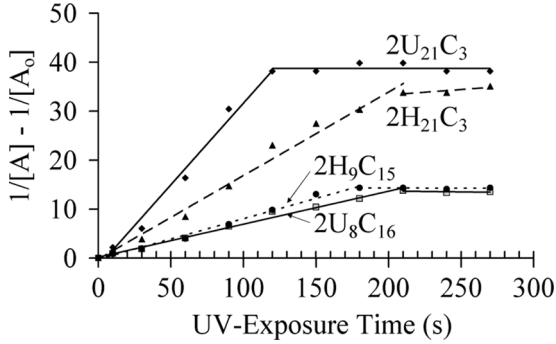

FIGURE 5 Kinetic plot investigating the rate of cinnamate photo-dimerization as a function of cinnamate and urethane concentration.

dimers. Confined side chains in the network structure prevented cinnamate groups from rearranging to fulfill the topotactic conformational requirements to achieve cinnamate dimerization [43]. The control sample, $2H_{21}C_3$, demonstrated the second fastest rate, $0.170\,s^{-1}$, and required 210 s of irradiation exposure to achieve a steady cinnamate concentration. $2U_8C_{16}$ and $2H_9C_{15}$ displayed similar rates of cinnamate dimerization, 0.069 and $0.081\,s^{-1}$, respectively. The cinnamate concentration of the control sample, $2H_9C_{15}$, and urethane sample, $2U_8C_{16}$, reached a steady state after 180 and 210 s of irradiation exposure, respectively. The increased rate of cinnamate dimerization with increasing concentration of urethane was not a consequence of chain mobility, due to the fact $2U_{21}C_3$ had the highest T_g, $-21^\circ C$.

A film of $2U_{21}C_3$ was spin cast onto a quartz slide from a 5 wt% toluene solution to examine the influence of film thickness on the rate of cinnamate dimerization. The 5 wt% rate of cinnamate photo-reactivity was compared with $2U_{21}C_3$ spin cast from a 10 wt% toluene solution. The influence of film thickness was examined to insure UV-radiation penetrated the entire thickness of the film affording uniform curing, and to explore the concentration effect on the exposure time required to reach a steady state of cinnamate concentration. The 5 wt% film was $0.18 \pm 0.12\,\mu m$ thick and the 10 wt% film was $1.02 \pm 0.13\,\mu m$ thick. The observed cinnamate dimerization rate of the 5 and 10 wt% films were very similar at 0.382 and $0.341\,s^{-1}$, respectively. The cinnamate concentration plateaued after 60 and 120 s of UV-irradiation for the 5 and 10 wt% films, respectively. As expected, the 5 wt% film achieved a steady cinnamate concentration faster because the film was thinner and contained a lower concentration of cinnamate groups.

Sol fraction analysis was conducted on urethane and control series films in refluxing THF. All non-cured films produced no gel fraction, and all UV-cured films were cured for 10 s with a measured UVB-dosage $0.147 \pm 0.05\,J/cm^2$. UV-cured films of $2U_{21}C_3$, $2U_{12}C_{12}$, and $2U_8C_{16}$ produced gel fractions of 25, 21, and 18%, respectively. Increasing urethane concentrations correlated to higher gel fractions for the urethane series, indicating the lowest molar concentration of cinnamate produced the highest gel fraction. The opposite effect was evident in the control series. Irradiated films of $2H_{21}C_3$, $2H_{12}C_{12}$, and $2H_9C_{15}$ produced gel fractions of 12, 15, and 19%, respectively. The gel fraction increased with increasing cinnamate groups for the control series. Increasing gel content with higher cinnamate concentrations was expected for compositions that did not contain hydrogen bonding groups [44].

CONCLUSION

A novel synergy combining hydrogen bonding and photo-reactive groups was developed in low T_g acrylic copolymers for application as HMPSAs. Acrylic copolymers of EHA, HEA, and MA were functionalized with urethane and cinnamate groups, and the reaction conditions were optimized to control the degree of functionality and manipulate the relationship between hydrogen bonding and photo-active sites. Hydrogen bonding associations provided strategies to increase the apparent molecular weight post-processing to prevent creep and cohesive failure. Processing above the hydrogen bonding dissociation temperature presents a methodology to maintain viscosities low for melt processing. Isothermal rheological experiments at 150°C confirmed the melt stability of the cyclohexyl urethane linkage, cinnamate, and the acrylic adhesive composition.

Precursors were functionalized with both urethane and cinnamate groups. The charged molar equivalence of cyclohexyl isocyanate to HEA determined the degree of urethane functionalization. All remaining residual HEA units of the urethane functionalized copolymer were reacted with cinnamoyl chloride introducing cinnamate functionality. The UV-cured peel strength increased as the concentration of urethane increased. Higher concentrations of cinnamates increased the T_g of the UV-cured film, preventing the adhesive from spreading and adequately contacting the substrate. All UV-cured films containing cinnamate groups failed 100% adhesively. Complete adhesive failure was attributed to the network formation from the intermolecular photo-dimerization of cinnamates. The percentage of adhesive failure for non-cured tapes increased as the concentration of urethane units increased. Increasing adhesive failure with urethane concentration was attributed to an increase in apparent molecular weight resulting from the intermolecular association of hydrogen bonding groups.

A control series was synthesized for comparison with the urethane series to investigate the influence of hydrogen bonding groups on the rate and efficiency of cinnamate photo-reactivity. The control series contained cinnamate groups and residual HEA units, and did not contain any urethane sites. The rate of cinnamate photo-dimerization as a function of composition comparing the urethane and control series was determined from a second order kinetic plot following the disappearance of conjugated cinnamates with UV-exposure, as shown in Figure 5. Both the urethane sample, $2U_{21}C_3$, and the control sample, $2H_{21}C_3$, contained three mole percent cinnamate with comparable molecular weights. Sample $2U_{21}C_3$ dimerized at a rate of $0.314\,s^{-1}$ and $2H_{21}C_3$ at a rate of $0.170\,s^{-1}$, indicating that the presence of

urethane groups assisted in the rate of cinnamate dimerization through the formation of intermolecular hydrogen bonds that confined the cinnamate groups in a proximity beneficial for photo-reactivity. The presence of the urethane was not influential when the concentration of the cinnamate group was increased for samples $2U_8C_{16}$ and $2H_9C_{15}$. The low concentration of urethane groups did not influence the rate of cinnamate photo-reactivity and the rate of dimerization was very similar for $2U_8C_{16}$ and $2H_9C_{15}$ at 0.069 and 0.081 s^{-1}, respectively. The relationship between urethane groups and cinnamate photo-reactivity provides evidence that high concentrations of hydrogen bonding associations can increase the efficiency of cinnamate photo-dimerization.

ACKNOWLEDGMENT

This material is work based upon funding from Avery Dennison Performance Polymers. We would like to acknowledge Mike Myers and Kevan Packard at Avery Dennison Chemical Division, Mill Hall, PA, for synthesizing the precursor copolymers.

REFERENCES

[1] Benedek, I., *Pressure-Sensitive Adhesives and Applications*, (Marcel Dekker, New York, 2004).
[2] Webster, I., *Int. J. Adhes. Adhes.* **17**, 69–73 (1997).
[3] Satas, D., *Handbook of Pressure Sensitive Adhesive Technology*, (Satas & Associates, Warwick, RI, 1999).
[4] O'Connor, A. E. and Macosko, C. W., *J. Appl. Polym. Sci.* **86**, 3355–3367 (2002).
[5] Czech, Z., *Polym. Bull.* **52**, 283–288 (2004).
[6] Sosson, F., Chateauminois, A., and Creton, C., *J. Polym. Sci., Part B: Polym. Phys.* **43**, 3316–3330 (2005).
[7] Czech, Z. and Wojciechowicz, M., *Eur. Polym. J.* **42**, 2153–2160 (2006).
[8] Qi, Y., Meng, X., Yang, J., Zeng, Z., and Chen, Y., *J. Appl. Polym. Sci.* **96**, 846–853 (2005).
[9] Everaerts, A., Zieminski, K., Nguyen, L., and Malmer, J., *J. Adhes.* **82**, 375–387 (2006).
[10] Dhal, P. K., Deshpande, A., and Babu, G. N., *Polymer* **23**, 937–939 (1982).
[11] Lim, D. H., Do, H. S., and Kim, H. J., *J. Appl. Polym. Sci.* **102**, 2839–2846 (2006).
[12] Kim, D. J., Kim, H. J., and Yoon, G. H., *Int. J. Adhes. Adhes.* **25**, 288–295 (2005).
[13] Benedek, I. (Ed.), *Pressure-Sensitive Design, Theoretical Aspects*, (VSP, Leiden, 2006).
[14] Ariga, K., Lvov, Y., and Kunitake, T., *J. Am. Chem. Soc.* **119**, 2224–2231 (1997).
[15] McKee, M. G., Elkins, C. L., Park, T., and Long, T. E., *Macromolecules* **38**, 6015–6023 (2005).
[16] Acierno, D., Amendola, E., Bugatti, V., Concilio, S., Giorgini, L., Iannelli, P., and Piotto, S. P., *Macromolecules* **37**, 6418–6423 (2004).

[17] Arumugam, S., Vutukuri, D. R., Thayumanavan, S., and Ramamurthy, V., *J. Am. Chem. Soc.* **127**, 13200–13206 (2005).
[18] Gower, M. D. and Shanks, R. A., *J. Polym. Sci., Part B: Polym. Phys.* **44**, 1237–1252 (2006).
[19] Dong, J., Ozaki, Y., and Nakashima, K., *Macromolecules* **30**, 1111–1117 (1997).
[20] Maurer, J. J., Eustace, D. J., and Ratcliffe, C. T., *Macromolecules* **20**, 196–202 (1987).
[21] Ren, Y., Pan, H., Li, L., Xia, J., and Yang, Y., *Polymer-Plastics Technology and Engineering* **45**, 495–502 (2006).
[22] Ansell, C. W. G., Masters, S. J., and Millan, E. J., *J. Appl. Polym. Sci.* **81**, 3321–3326 (2001).
[23] Asahara, J., Hori, N., Takemura, A., and Ono, H., *J. Appl. Polym. Sci.* **87**, 1493–1499 (2003).
[24] Berejka, A. J., *Adhes. Age* **40**, 30–32, 35–36 (1997).
[25] Czech, Z., *Eur. Polym. J.* **40**, 2221–2227 (2004).
[26] Yang, S. Y. and Rubner, M. F., *J. Am. Chem. Soc.* **124**, 2100–2101 (2002).
[27] Kim, C., Lee, S. J., Lee, I. H., Kim, K. T., Song, H. H., and Jeon, H. J., *Chem. Mater.* **15**, 3638–3642 (2003).
[28] Yang, D. K., Chien, L. C., and Doane, J. W., *Appl. Phys. Lett.* **60**, 3102–3104 (1992).
[29] Karikari, A. S., Edwards, W. F., Mecham, J. B., and Long, T. E., *Biomacromolecules* **6**, 2866–2874 (2005).
[30] Karikari, A. S., Williams, S. R., Heisey, C. L., Rawlett, A. M., and Long, T. E., *Langmuir* **22**, 9687–9693 (2006).
[31] Barwich, J., Dusterwald, U., Meyer-Roscher, B., and Wustefeld, R., *Adhes. Age* **40**, 22–24 (1997).
[32] Fukui, H., Ishizawa, H., and Nakasuga, A., *J. Photopolym. Sci. Technol.* **12**, 169–172 (1999).
[33] Robertson, E. M., Van Deusen, W. P., and Minsk, L. M., *J. Appl. Polym. Sci.* **2**, 308–311 (1959).
[34] Kimura, T., Kim, J. Y., Fukuda, T., and Matsuda, H., *Macromol. Chem. Phys.* **203**, 2344–2350 (2002).
[35] Fang, S. W., Timpe, H. J., and Gandini, A., *Polymer* **43**, 3505–3510 (2002).
[36] Gheneim, R., Perez-Berumen, C., and Gandini, A., *Macromolecules* **35**, 7246–7253 (2002).
[37] Zahir, S. A., *J. Appl. Polym. Sci.* **23**, 1355–1372 (1979).
[38] Trenor, S. R., Shultz, A. R., Love, B. J., and Long, T. E., *Chem. Rev.* **104**, 3059–3077 (2004).
[39] Murase, S., Kinoshita, K., Horie, K., and Morino, S., *Macromolecules* 30, 8088–8090 (1997).
[40] Aharoni, S. M., *Macromolecules* **19**, 426–434 (1986).
[41] Chae, B., Lee, S. W., Ree, M., Jung, Y. M., and Kim, S. B., *Langmuir* **19**, 687–695 (2003).
[42] Sung, S. J., Cho, K. Y., Yoo, J. H., Kim, W. S., Chang, H. S., Cho, I., and Park, J. K., *Chem. Phys. Lett.* **394**, 238–243 (2004).
[43] Darcos, V., Griffith, K., Sallenave, X., Desvergne, J. P., Guyard-Duhayon, C., Hasenknopf, B., and Bassani, D. M., *Photochemical & Photobiological Sciences* **2**, 1152–1161 (2003).
[44] Gupta, P., Trenor, S. R., Long, T. E., and Wilkes, G. L., *Macromolecules* **37**, 9211–9218 (2004).